Transportation Research Part C 109 (2019) 19–39

Contents lists available at ScienceDirect

Transportation Research Part C

journal homepage: www.elsevier.com/locate/trc

Collision risk management for non-cooperative UAS traffic in airport-restricted airspace with alert zones based on probabilistic conflict map

C.H. John Wang[b,1], Shi Kun Tan[b,1], Kin Huat Low[a,*]

[a] School of Mechanical and Aerospace Engineering, Nanyang Technological University, Singapore 639798, Singapore
[b] Air Traffic Management Research Institute, Nanyang Technological University, Singapore 637460, Singapore

A B S T R A C T

Recent years have seen an increase in reported unmanned aerial systems (UAS) incursion into terminal airspace, likely due to the ease of access to recreational UAS to the general public with minimal understanding of aviation regulations. Such incursions often lead to extensive airport shut-downs due to safety concern and could cause a cascading disruption to airline operations throughout the region. A better assessment tool for the collision risk between the existing air traffic and such non-cooperative intruder could help reduce unnecessary disruption while maintaining safety to air traffic operations. While advancements have been made in the past decade in detection and avoidance of UAS traffics, the systems depend on either having fully cooperative traffic or sensor capability beyond what is currently available. This paper seeks to assess the collision risk posed by an intruding UAS within the airport-restricted "terminal airspace," in the Singapore context, with minimal information on the UAS. This was done through probabilistic conflict prediction with Monte-Carlo simulations under the assumption of a worst-case scenario involving a non-cooperative intruder traveling directly towards the flight corridor. Alert Zones within the existing 5 km terminal airspace could be constructed using the collision prediction models to help air traffic controllers quickly identifying UAS that poses a threat under most circumstances, with the information passed on to the pilot for mitigation actions. Simulations were conducted for a number of conflict-pairs to investigate how the resulting Alert Zones differ. Finally, this paper also investigates how the incorporation of UAS tracking information, under the current reliability level, could be used to augment the collision prediction algorithm and its effect on the management of collision risks in terminal airspace. The result suggested that the method that utilizes the most available information for UAS path modeling could be used with the currently available sensors to produce acceptable collision prediction results.

1. Introduction

The rapid development of recreational multi-copter in recent years has enabled the general public to access the unmanned aerial systems (UAS), whether recreational or professional grade, through a wide range of manufacturers and at an affordable rate. These UAS, like the radio-controlled (RC) aircraft from the previous generations, does not require the operator to possess a license issued by the aviation authorities; however, comparing to the older generation of RC aircraft, the multi-copter is both cheaper to purchase and easier to operate. With the influx of inexperienced UAS operators with little knowledge of aviation regulations, a rising number incidents where UAS intrude into restricted airspace has been reported (Michel et al., 2015). The hazard posed by these UAS intrusion, and the possible damage caused, is especially high in the terminal airspace around the airport where passenger aircraft operates at low speed and low altitude. An incursion into the terminal airspace by a UAS would often lead to extended airport shutdowns. These shutdowns could last for as long as a few hours, depending on how soon the hazardous UAS could be removed from

* Corresponding author at: 50 Nanyang Avenue, Singapore 639798, Singapore.
E-mail address: mkhlow@ntu.edu.sg (K.H. Low).
[1] 65 Nanyang Drive, Singapore 637460, Singapore.

https://doi.org/10.1016/j.trc.2019.09.017
Received 25 August 2018; Received in revised form 19 July 2019; Accepted 20 September 2019
Available online 24 October 2019
0968-090X/

the airspace or could be reasonably assumed to no longer pose a threat (Deulgaonkar, 2017; BBC News, 2017; George, 2018). The knock-on effect of such shutdown on airport operation and airline scheduling could last for days afterward.

With the operation of larger UAS (>7 kg) in Singapore heavily regulated (Air Navigation Order, 2018), requiring both a valid license from the pilot as well as an approved flight plan, the likelihood of intrusion by this type of UAS is slim. On the other hand, recreational UAS (<7 kg) could be operated freely as long as it stays under 200 ft (~61 m) above mean sea level (AMSL) and outside of the designated restricted airspace. However, the monitoring and enforcement of these restrictions could be difficult. Without the need of a licensed operator and to file a flight plan the recreational UAS, which lack the traceability and accountability compared to the larger commercial UAS, could pose a higher risk of terminal airspace incursion in Singapore.[2]

Currently, the prevention of unintentional incursion into controlled airspace by recreational UAS operators is achieved through global positioning system (GPS) based geofencing that is a part of the flight controller. The database for these controlled airspace is usually maintained by the manufacturers, and would often require the operator to sync with the central database before each flight. However, geofencing would not work if the UAS does not have the geofenced area in its database, either due to the lack of data connection for database update or the malfunctioning of flight controller; it would also not work for a UAS with legacy or open source flight controller that does not contain the relevant system to enforce geofencing. In such case, the wayward UAS would need to be treated as non-cooperative traffic by the air traffic controllers (ATC), as there would be no way for them to interact with the intruding UAS and coordinate actions required to avoid interference with airport operations.

For cases where the incursion of the UAS is not preventable by existing means, the aim of the collision prevention algorithm would then be on ensuring the safety of the existing aircraft operating in the controlled airspace for the duration needed to complete their takeoff or landing operations. The first goal for this study is to establish Alert Zones within the terminal airspace using collision risk modeling to quickly assess the threat level of the intruding UAS to aircraft already in operation within the terminal airspace; this is conducted with the currently available airport infrastructure in mind. The second is to investigate the impact of ground-based sensor data availability, as well as the amount of information available, on those collision risk assessments; the investigation would compare the collision risk predicted with different models and the associated probability of failure. The simulation algorithms and methodologies in this study follows those presented in our previous conference paper (Wang et al., 2018).

2. Literature review

Collision prevention between aircraft is generally handled by the air traffic controllers who would spot possible conflict through the usage of secondary surveillance radar, which obtain the aircraft positions through their ADS-B transponder broadcast; the ADS-B transponder has an update interval 3 s or less (FAA, 2014). In the rare cases where the ATC did not notice the aircraft pair getting too close to each other, the Airborne Collision Avoidance System (ACAS) would act as a fail-safe to prevent a possible collision. The ACAS accomplishes this by utilizing specialize equipment that broadcast the position of the host aircraft and identifies other ACAS equipped aircraft that is on a collision course; the update interval for ACAS II standard is 1 s. The system then provides a warning to the pilots on the incoming traffic and would issue a resolution advisory if no corrective action was taken after a period of time (EUROCONTROL, 2016). The specific implementation of ACAS II standard on civil aviation aircraft is the TCAS (Traffic Collision Avoidance System) II, of which version 7.0 and 7.1 are the only two equipment in full compliance with the ACAS II standard at this time.

In air traffic management, aircraft that is able to broadcast its position and receive the position of others in the area, either through ACAS type transponder/receiver equipment or coordinated by local ATC, are called cooperative traffic. On the other hand, aircraft that lack either, or both, of these functionalities would be called non-cooperative traffic. Thus, a UAS operating in the terminal airspace without direction communication between the operator and the ATC, such as the case of intrusion by recreational UAS, would be considered as non-cooperative air traffic even if the UAS could be detected by the ATC or the pilots.

2.1. Detecting non-cooperative traffic

One of the ways to detect and track non-cooperative air traffic is through the usage of ground-based primary radar, which is effective for general aviation aircraft or larger, while other sensors might be required for smaller flying objects due to radar wavelength and the resolution. The ground-based detection of intruding UAS could be accomplished using a number of active and passive detection technologies: Active detection of UAS is generally achieved using Pulse-Doppler radar, while the passive detection technologies utilize receivers to capture the energy reflection/emission from the UAS, e.g. camera for visible/IR light reflections, radio spectrum sensor for controller transmissions, or acoustic sensor for noise emissions. Each of the detection method has its own strengths and weaknesses, such as a camera is cheap to install, but its detection ability suffers under low visibility conditions, thus limiting its effective detection range. A report published in 2012 by the Netherlands Aerospace Center (NLR) concluded that the ground-based sensors available at the time is unable to provide the equivalent level of safety compared to that of the manned aviation (Verstraeten et al., 2012). More recently, the Massachusetts Department of Transportation reviewed eight ground-based systems available on the market (Looze et al., 2016), and found only four of those were capable of covering the 5 km controlled airspace surrounding the runway. The systems were shown to have a maximum detection probability of 0.99, or a probability of failure at 10^{-2}, far from sufficient for civil aviation applications.

[2] The “terminal airspace” here on referred to the 5 km restricted airspace surrounding an airport (Singapore Air Navigation Order Part XA, §72D(c)(ii).) would be referred to as the “terminal airspace” in the rest of the article.

Without the UAS detecting equipment, the ATC would have to depend on sighting reports, either from the pilots or the airport ground crew, to recognize that a UAS incursion occurred. These reports might consist of only the estimated flight performance of the UAS (based on the type of UAS e.g. recreational UAS or payload capable commercial UAS) and a rough position of its initial incursion. Based on the reported initial conditions, the collision risk assessment could be calculated either based on the estimated closest-point-of-approach (CPA) similar to the approach used for the ACAS (EUROCONTROL, 2016) or the collision prevention system used in UAS obstacle avoidance algorithm (Angelov, 2012; Kim et al., 2007). However, the margin of error in UAS collision forecast is expected to be quite high due to the uncertainties involved.

2.2. Avoiding airborne traffic conflicts

The modeling of the collision risk posed by non-cooperative traffic in terminal airspace follows a similar procedure as the UAS detect-and-avoid (DAA) research (Angelov, 2012), which has its root in the research done to develop the current generation of ACAS equipment (Krozel et al., 1997). The avoidance of airborne traffic conflict would involve the following steps: detection of traffic, propagation of states, detection of conflict, and resolution of the conflict (Kuchar and Yang, 2000).

Comparing to the present study, recent developments on DAA for non-cooperative UAS are mostly focused on either step one, the detection and traffic recognition capability of the UAS to achieve autonomous operation (through optical sensors for small UAS (Feng et al., 2018; McFadyen et al., 2016) or multi-sensor fusion for large UAS (Fasano et al., 2008; Fasano et al., 2015)), or step four, the conflict resolution and traffic management with the assumption that traffic detection could be achieved reliably through mapping of airspace to avoid for a UAS pair in conflict (Tony et al., 2017), vertical maneuvers (Cone et al., 2017), or using deep learning to generate conflict resolution maneuvers (Chen et al., 2017).

The conflict evaluation workflow bears some similarity to the Reich Collision Risk Model, which is the process of designing air routes in close-parallel crossing pattern and the associated separation requirement for cooperative traffic (ICAO, 1998). In this case, the initial conditions of the crossing traffic could be obtained with the available navigation equipment available for the operating airspace. The probability of conflict was evaluated over the reporting period using a combination of probability of aircraft overlap due to navigational system error, the initial relative difference in velocity of the “host” and “traffic”, and the along-track traffic density. The separation requirement for a given airspace with known Required Navigational Performance (RNP) could then be obtained by going through a range of initial separation distances for that particular cooperative aircraft pair. Furthermore, the methodology used for lateral and longitudinal collision risk assessment could be adapted to utilize existing or estimated traffic statistics between point of interests or navigation waypoint to estimate the network-wide collision risk in air route planning for both civil aviation (ICAO, 1998) and future integration of UAS traffic (McFadyen and Martin, 2016; Peinecke and Kuenz, 2017; Weinert and Underhill, 2018).

For non-cooperative traffic in terminal airspace, the traffic detection would be based on sighting reports by the ground crew; the simulation tool would perform the propagation of states, i.e. intruder path prediction, and detection of potential conflict. If a possible conflict is predicted, the ATC would then notify the pilot of the manned aircraft operating inside terminal airspace on the direction to search for the intruder. The pilot-in-control would then decide, based on available information at the time, the appropriate action to maintain flight safety either by maintaining visual separation with the intruder or by aborting the takeoff/landing operation. The recommendation of action to resolve the conflict is not covered in the scope of this study. The following sections outline existing works on the state propagation and conflict detection for airborne traffic.

2.2.1. Aircraft state propagation

Predicting the range of possible future position of the aircraft is generally conducted through three different methods in ACAS related research, illustrated in Fig. 1: the nominal (intention) based prediction, the worst-case (maximum range) based prediction, and the probabilistic based prediction (Krozel et al., 1997; Kuchar and Yang, 2000). The nominal method assesses the collision risk by extrapolating the aircraft trajectories of both the host and the incoming traffic by maintaining the current velocity and direction of the two aircraft; the worst-case method predicts collision by evaluating the possible intersection of the volume of motions of the two

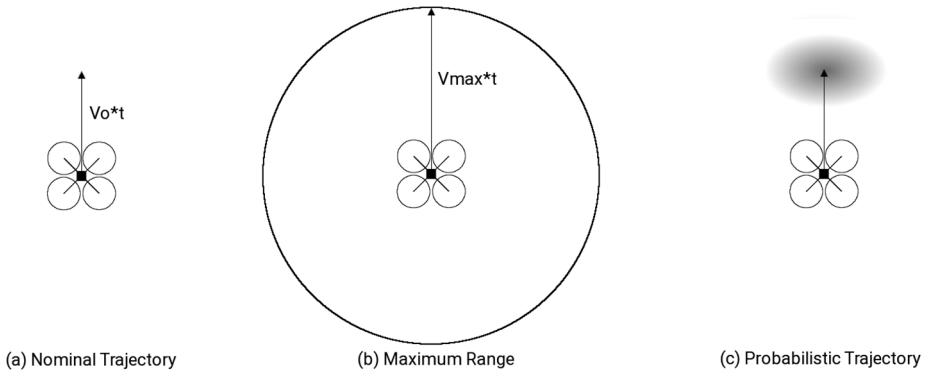

Fig. 1. Common trajectory prediction methods: (a) Nominal, (b) Worst-Case, and (c) Probabilistic methods.

aircraft, which is defined by their maximum range of motion; the probabilistic method could be achieved through several approaches: by applying a probabilistic distribution around a future aircraft position calculated using the deterministic approach (Paielli and Erzberger, 1997; Taylor, 1990; Carpenter and Kuchar, 1997); by running Monte-Carlo simulation from a known initial position to obtain the final positional distribution (Krozel et al., 1997); or by a combination of both by updating the initial conditions for the Monte-Carlo simulation using new sensor data as it becomes available (Yang and Kuchar, 1998; Kim et al., 2007).

The new version of ACAS currently under development, the ACAS X, also utilizes the probabilistic state estimation for the detecting conflict (EUROCONTROL, 2016). This is performed using dynamic programming instead of Monte-Carlo simulation, which assign a probability to a state similar to the approach taken in Ref. (Paielli and Erzberger, 1997; Taylor, 1990; Carpenter and Kuchar, 1997). More specifically, the aircraft state was defined using a Bayesian Network where the probability for each state variables evaluated from historical track statistics using several categories, e.g. the airspace category and aircraft type (Kochenderfer et al., 2010; Kochenderfer and Chryssanthacopoulos, 2011; Muller and Kochenderfer, 2016; Weinert et al., 2012). Like its predecessor, ACAS X does not provide protection against non-cooperative intruders, though ACAS Xu for installation on UAS requires on-board sensors to be equipped for non-cooperative intruder detection (Davies and Wu, 2013).

In the case of non-cooperative UAS with no available tracking information, path prediction would not be possible using the nominal method and the deterministic approach; the aircraft/UAS tracks would also be considered as uncorrelated. The usage of maximum UAS reach was also ruled out for the multi-rotor UAS due to its high maneuverability; the maximum range of the UAS would simply show up as a sphere with the radius based on the maximum UAS flight range. That leaves the probabilistic method that utilizes either characteristics extracted from existing flight path data (Weinert et al., 2012; Muller and Kochenderfer, 2016; Wallace et al., 2018a) or Monte-Carlo Simulation (Wang et al., 2018). One of the limitation of the flight path characteristics method is that it could be vehicle type, airspace class, and region dependent, i.e. path data from the US would not be applicable in Singapore, and the dataset available might not be representative for the situation being investigated (Wallace et al., 2018a). The method was also not designed to capture malicious or hobbyist operations (Weinert et al., 2018b), thus not suitable for safety critical application where the off-nominal and malicious cases would need to be considered.

2.2.2. Collision detection

Once the state-propagation method was chosen, it could be used to determine the expected position, or the distribution of the probable positions, of the “host” aircraft and the intruding UAS over time. This could be used to calculate the distance between the two aircraft at the closest point of approach (CPA) that could be, in the case of ACAS II, compared to a distance criterion to determine if it would breach the protected volume of the “host” aircraft (EUROCONTROL, 2016). The distance criterion used would depend on the type of aircraft and airspace involved (Duffield and McLain, 2017), and could range from the half-span of the aircraft (Metz et al., 2017; ICAO, 1998) or the Near Mid-Air Collision (NMAC) distance (Lee et al., 2013) to several nautical miles around the reported position of the aircraft (Krozel et al., 1997; Cook et al., 2015; ICAO, 1998). However, the most utilized criterion for collision prediction for is adapted from that used in the ACAS II, either for manned aircraft encounters (Weinert et al., 2012) or UAS-centric encounter pairs (Lee et al., 2013; Johnson et al., 2015; Cook et al., 2015).

The selection of distance criterion, sometimes referred to as the Well-Clear distance, that defines the protected volume depends on the types of aircraft in conflict and the scenario that is being considered. For example, in the bird strike risk simulation by Metz et al. (2017) both the position of the aircraft and the modeled distribution of the bird flock are treated as their true position, thus only the half-span of the aircraft was used to generate the protected volume. In the Reich CRM (ICAO, 1998), the positions of the aircraft in conflict are their reported positions, which requires the model to account for the navigational uncertainties. The distance criterion in ACAS II-based systems took it a step further and considered the time needed to perform vertical de-conflicting maneuvers (EUROCONTROL, 2016; Duffield and McLain, 2017; Muñoz et al., 2014).

Several factors were considered in determining the dimension for different layers of the ACAS II protected volume (EUROCONTROL, 2016), which was developed based on ANTC-117 (Bagnall and Kay, 1975): the inner most layer, defined by the distance modifier (DMOD), is the distance required for the “host” aircraft to achieve an altitude change with $a_z < 1/4g$ that clears the vertical threshold (ZTHR) regardless of the rate of approach from the intruder; the second layer for resolution advisory (RA) included the relative position and approach rate at the time, which were used to calculate the time to closest approach τ_{RA} and the distance required to accomplish the same escape maneuver; the final layer for traffic advisory (TA) would give the pilot an additional 10–15 s of reaction time to prepare for the possible RA, though an RA might not necessarily be preceded by a TA.[3] Note that for traffic with low approach rate the τ value could approach infinity, at which point the DMOD boundary would be used instead. Additionally, the RA function is inhibited at low altitude due to terrain, and only the TA would be issued.

More recently, works have been done on the evaluation of Well-Clear definition for the UAS as the “host” aircraft to facilitate the integration of UAS into the overall air traffic management system (Muñoz et al., 2014; Johnson et al., 2015). The UAS Well-Clear definition studies aimed to address the ambiguous Well-Clear definition for manned visual-flight-rule traffic where separation is maintained based on the pilot’s judgment, but largely follows the criterion used in ACAS II for low altitude traffics (Lee et al., 2013; Muñoz et al., 2014; Cook et al., 2015; Duffield and McLain, 2017). Encounter models using probabilistic traffic path based on representative historical traffic data are often used to evaluate the effectiveness of these definitions. However, for low level operation the risk contours for small UAS encounter with manned aircraft showed a lack of sensitivity to the aircraft type and encounter model (Weinert et al., 2018b).

[3] The values for DMOD, ZTHR, τ_{TA}, and τ_{RA} depend on the altitude of the aircraft, and are listed in Table 6 in Ref. (EUROCONTROL, 2016).

3. Modeling strategies

The setup for the establishment of the Alert Zones for terminal airspace took inspiration from the potential conflict maps from Ref. (Yang and Kuchar, 1997; Yang and Kuchar, 1998; Krozel et al., 1997), which shows the probability of conflict posed by the intruder aircraft at various initial position. The probability of conflict for each intruder initial position was evaluated using the ratio between the number of Monte-Carlo samples that intrude into the protected airspace of the host aircraft and the total number of intruder aircraft samples simulated. The Monte-Carlo simulations were carried out using the reported speed and position of both aircraft as initial conditions and the aircraft performance as constrains to the range of motion. The conflict map could be produced with the assumption that both the host and intruder aircraft maintain current course (Yang and Kuchar, 1997; Krozel et al., 1997) or performs prescribed horizontal escape maneuvers (Yang and Kuchar, 1998).

For the purpose of this study, the commercial/civil aviation aircraft operating in the terminal airspace would be treated as the "host" in the conflict scenario. The position of the aircraft is assumed to be known to the ATC, and follows the established takeoff and approach track of the airport at the published takeoff/landing speed. The reported position of the aircraft is assumed to have minimal deviation from the prescribed path based on historical data (Hall and Soares, 2008; Zhang et al., 2010). The simulation was modeled only in 2D due to the vertical dimension of the ACAS II protected volume for aircraft operating within the 5 km terminal airspace, which is 850 ft (~260 m) above and below the reported altitude of the aircraft operating at < 1000 ft Above Ground Level (AGL).

Modeling of the intruding UAS is complicated by the lack of information about the intruder available to the pilot of the host aircraft and the air traffic controller. Using the assumption that the intruding UAS is non-cooperative and the airport is not equipped with sensors for UAS detection, the initial position of the UAS would have to come from sighting reports, which might also contain the size and flight mechanism of the UAS. Furthermore, the intended direction of travel for intruder would not be available, thus the only constraint on intruder range of motion is its flight envelope, which were modeled after quad-rotors using the kinematic equation of motion. Section 3.1 outlines the implementation of the kinematic equation to model the probabilistic distribution of the intruder, and Section 3.2 discuss the construction of protected volume to be used in collision prediction. Together, the predicted distribution of the intruder and the associated collision probability over a range of initial positions could be used to create the Alert Zone for UAS incursion in the 5 km terminal airspace around the airport.

3.1. Path prediction

Monte-Carlo simulation is a method to obtain the probabilistic distribution of the output from a complex system with randomized input. In this case, the complex system is the process that leads up to the position of the UAS by the end of the simulation time while an input variable would be randomized at the beginning of each time step. For each time-step, the resulting movement of the UAS would need to be check against the kinematic equation to ensure that movement could be made physically. Since the UAS is modeled as a quad-rotor and limited to 2D motion in this simulation, the vertical thrust component must be equal in magnitude to its weight. The acceleration of the UAS could then be computed using the remaining thrust available and the drag force acting on the UAS, where the drag constant K_d were set such that the drag force equals the maximum available thrust when the UAS is traveling at the maximum speed. Assuming that the model of the intruding UAS and its initial velocity are known, the acceleration, velocity, and the position of the UAS could be computed for the end of that time-step using just one randomization function on the thrust vector. The resulting, simplified equation of motion for the UAS is given by

$$\boldsymbol{a} = \frac{d\boldsymbol{V}}{dt} = \frac{(\mathcal{X}\boldsymbol{T_{max}} - m\boldsymbol{g} - K_d\boldsymbol{V_0^2})}{m} \tag{1}$$

where $\mathcal{X}\boldsymbol{T_{max}}$ is the randomized 3D thrust vector that acts as an analogue of the fluctuation in speed and direction of the UAS. Its magnitude is bounded between the weight of the UAS ($m|\boldsymbol{g}|$) and the maximum thrust of the UAS $|\boldsymbol{T_{max}}|$. The acceleration $\boldsymbol{a}$ is assumed to be constant for the given time-step, while $\boldsymbol{V_0}$ is the velocity vector at the beginning of the time-step. Note that due to the 2D motion assumption the vertical component of both $\boldsymbol{a}$ and $\boldsymbol{V_0}$ are equal to zero, while $|\boldsymbol{T_{max}}| \geqslant |m\boldsymbol{g}|$ is required to enforce the constant altitude. The drag constant does not change throughout the simulation, and is obtained through $K_d = \sqrt{|\boldsymbol{T_{max}}|^2 - m^2|\boldsymbol{g}|^2}\,/|\boldsymbol{V_{max}}|^2$ which prevents the UAS from accelerating above its maximum speed.

More specifically, the random distribution ($\mathcal{X}$) could be implemented using a number of built-in random number generators that produce values bounded by the available thrust. For example, for a UAS only flying in the Y-direction with uniform thrust distribution, the random number generator would be $\mathcal{X}\sim\mathcal{U}(-1, 1)$ and the available thrust would be $T_{y,max} = \sqrt{|\boldsymbol{T_{max}}|^2 - m^2|\boldsymbol{g}|^2}$ where $|\boldsymbol{T_{max}}| \geqslant |m\boldsymbol{g}|$. Similarly, for the same UAS with Gaussian (normal) distribution for the randomized thrust and a standard deviation of $\sigma = 20\%$ (variance $\sigma^2 = 0.04$) of the maximum value $|T_{y,max}|$ and a prescribed target thrust value $|T_{target}| \leqslant |T_{1D,max}|$ as mean. Thus, the random number generation term would be $\mathcal{X}\sim\mathcal{N}(|T_{target}|/|T_{y,max}|, 0.04)$ and truncated between [-1,1]. For 2D motion, the thrust value in the longitudinal (y) direction is first generated and the leftover thrust, $(1 - \mathcal{X})|T_{y,max}|$, is used to generate the lateral (x) thrust value for that time step. Once both components of the thrust vector have been generated, this value could be used to compute the acceleration for each of the Monte-Carlo samples using the following equation:

$$\boldsymbol{x} - \boldsymbol{x_0} = \frac{1}{2}\boldsymbol{a}\Delta t^2 + \boldsymbol{V_0}\Delta t \tag{2}$$

where $\boldsymbol{x}$ is the initial and $\boldsymbol{x_0}$ is the final position of the sample.

An example of the 2D UAS distributions using the uniform random number generator and the process described above is shown in

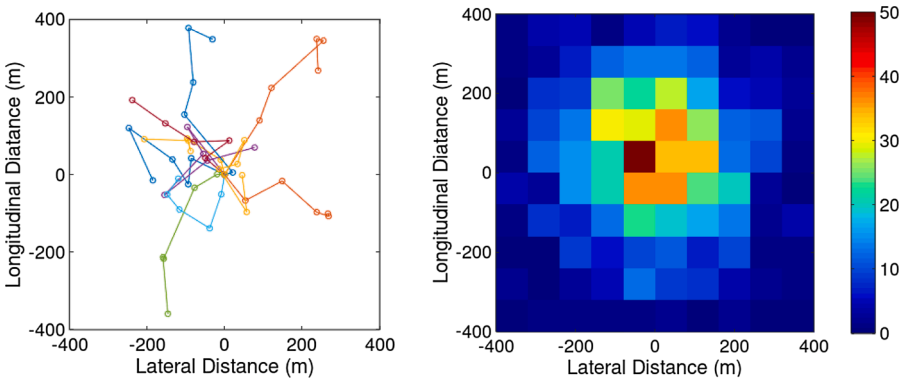

(a) Sample Paths (b) Histogram

Fig. 2. Path prediction using the uniform-random algorithm showing (a) sample paths and (b) histogram from 1000 samples using Monte-Carlo simulation. Simulation time of 100 s and V_{max} of 20 m/s was used.

Fig. 2. The UAS used for the simulation is based on the DJI Inspire 2, which is the largest off-the-shelf flyable UAS from one of the largest recreational UAS manufacturer with a total mass of under 7 kg. The performance data of the Inspire 2 is listed in Table 1.

Fig. 2(a) depicts 10 sample paths recorded over the course of the simulation at 20 s interval, while Fig. 2(b) is the 2D histogram showing the distribution from 1000 Monte-Carlo samples by the end of the simulation. The simulations were conducted with a constant time-step size of 0.2 s and an initial velocity of 26 m/s in the positive-longitudinal direction.

The Monte-Carlo results for uniformly random thrust input showed that >90% of the samples were located within 350 m of the origin by the end of the 100 s simulation. In other words, it would take well over 1×10^{12} samples to capture a Monte-Carlo sample with end-position near its maximum range of 2600 m. In fact, it would take the random number generation to output the same number (1 for longitudinal and 0 for lateral) for every time-step for a sample to reach its maximum range. Instead of the uniform random number generator, the normal random number generator using those output value as mean could capture the edge case, using significantly lower sample count, where the UAS is prescribed an intention to travel towards the aircraft flight path with the maximally available thrust. Simulations with such "assumed intent" would allow the assessment of probabilistic collision risk under a worst-case scenario while accounting for some random variation in vehicle movement. Table 2 shows the Jackknife re-sampling (Miller, 1974) result for the "assumed intent" case with different Monte-Carlo sample sizes.

Given the computation time required and the bias observed, the sample size of 2000 was chosen for the subsequent simulations. Additionally, the difference between simulations conducted using uniform random number generator and the prescribed "intent" using the normal random number generator is demonstrated in Fig. 3 over a period of 200 s with 2000 samples each. The mean range of the UAS samples with prescribed "intent" is 4680 m compared to the absolute maximum range of the UAS (5200 m), while the mean from the uniform random simulation is zero.

The simulation results from Fig. 3(b) resembles the distribution shown in Ref. (Yang and Kuchar, 1998; Paielli and Erzberger, 1997), which were generated using Monte-Carlo simulation on fixed wing aircraft. A larger variation in the lateral direction observed in the current case is likely due to the difference in maneuverability between the fixed-wing civil aviation aircraft and the multi-rotor UAS. Note that the "intent" assumption (applying maximum thrust and traveling towards the flight corridor) must be applied to the random number generator at each time step, and not just the initial condition. Otherwise, the result after enough time-steps would eventually resemble that of the uniform random number generator.

3.2. Collision prediction

The collision risk calculation in this study follows earlier Monte-Carlo based collision prediction studies (Yang and Kuchar, 1997; Krozel et al., 1997; Yang and Kuchar, 1998), and evaluate the probability of collision by evaluating the percentage of Monte-Carlo samples that falls within the "protected volume" surrounding the host aircraft. Several protected volume designs for collection

Table 1
Performance specifications of DJI Inspire 2, from Ref. (DJI Technology Co., Ltd, 2017).

Variable	Value
Maximum Thrust ($\|\boldsymbol{T_{max}}\|$) [a]	8 kgf
UAS Mass (m)	3.4 kg
Maximum Speed ($\|\boldsymbol{V_{max}}\|$)	26 m/s

[a] 2 kg per rotor (Inspire 2, 2019), not stated in the manual.

Table 2
Jackknife Bias Statistics for Various Monte-Carlo Sample Sizes from the Assumed "Intent" Simulation Setup.

Sample	E-W Direction Bias (m)		N-S Direction Bias (m)	
Size	Mean	σ	Mean	σ
100	0.000	-0.229	-6.753×10^{-11}	-2.358×10^{-2}
1000	-1.331×10^{-12}	-2.103×10^{-2}	-1.136×10^{-9}	-1.588×10^{-3}
2000	-5.326×10^{-12}	-1.148×10^{-2}	1.364×10^{-9}	-7.346×10^{-4}
5000	-4.440×10^{-12}	4.2×10^{-3}	0.000	-2.999×10^{-4}

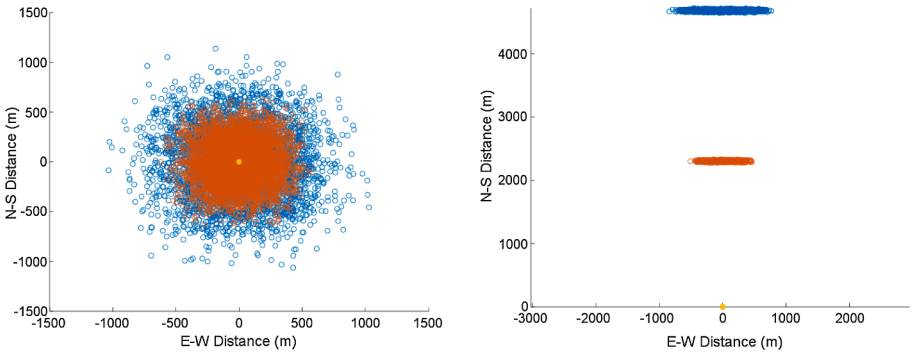

(a) Without intent assumption (b) With intent assumption

Fig. 3. Projected position of the UAS as it spread out over time, using (a) the uniform-random algorithm (without intent assumption) and (b) the normal distribution with variance of 1, i.e. with intent assumption. The symbols are: initial UAS position (solid yellow circle), 100 s predictions (orange circle), and 200 s predictions (blue circle) using 2000 samples. (For interpretation of the references to colour in this figure legend, the reader is referred to the web version of this article.)

detection were reviewed in Section 2.2.2, with each of the protected volume requiring different level of confidence with the "host" and "traffic" positions. The ACAS II based model was chosen for the current study due to the similarity in the associated availability of aircraft information, i.e. the "host" aircraft position based on its reported position and the "traffic" based on the modeled "true" position of the UAS.

The ACAS II protected volume for collision prediction inside the terminal airspace where the aircraft travel at lower altitude (< 1000 ft AGL) and slower speed would consist of two layers, the first is the Traffic Advisory (TA) layer (τ = 20 s to collision) and the minimum distance required for escape maneuver (DMOD = 0.3 nautical miles), referred in this study as the Collision Area (CA) zone. A similar two-layer approach was also used in a 2013 conceptual document for Low Altitude Conflict Monitor as a part of Next Generation Air Transportation Systems concept (Otero et al., 2013). The protected zones implemented in this paper follows the criterion from the ACAS II regulations, as illustrated in Fig. 4, but could be changed in the future as new regulations are put in place.

Since the calculation of τ is based on the maximum speed of the incoming traffic, it was assumed that the model of the "traffic" UAS, hence its maximum speed, is available from the sighting report. Note that the TA volume for UAS collision case does not extend to the rear half of the host aircraft due to the difference in travel speed: the host aircraft typically travels at a landing speed of 140 knots (~72 m/s) or a takeoff speed of 155 knots (~80 m/s), while the UAS used in this study has a maximum speed of 26 m/s. One of the factors that led to the decision to conduct a 2D simulation instead of 3D was due to the size of the protected volume in the vertical direction. The minimum vertical separation in ACAC II, once the intruding aircraft is determined to have intruded into the horizontal protected zone, for a host aircraft operating at <1000 ft AGL is 850 ft. This would cover almost the entire space between 1850 ft AGL to the ground.

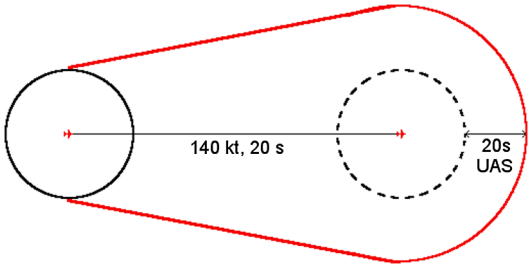

Fig. 4. Traffic Advisory (TA) zone (red lines) and the collision area (CA) zone (solid black circle) of an aircraft.

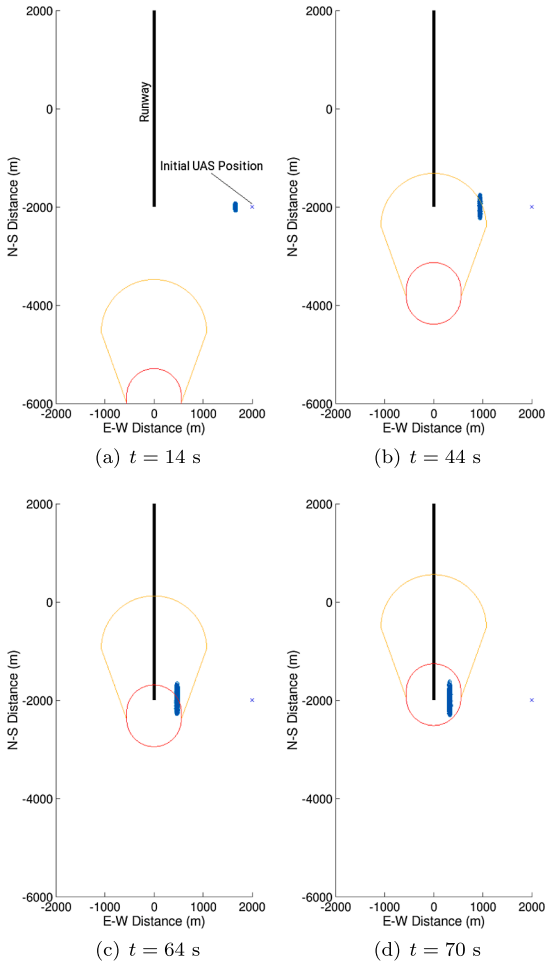

Fig. 5. A sample case showing the collision risk simulation, at (a) 14 s when the aircraft entered into the frame, (b) 44 s, triggering TA warning with 93.7% of samples inside TA zone, (c) 64 s, collision predicted with 62.5% of samples inside CA zone, and (d) 70 s, with 100% of the samples inside CA zone.

A sample case of the collision assessment with a landing aircraft and a UAS with initial position of (2000,-2000), with the mid-point of the runway as (0,0), is shown in Fig. 5. A total of 2000 samples were used in the simulation over a period of 70 s with the assumption that no external factors were involved. The simulation showed that 93.7% of the UAS samples would intrude into the TA zone at $t = 44$ s, thus triggering the TA alert, and a collision is predicted to occur at $t = 64$ s with 62.55% of samples falling inside the CA zone.

4. Results and discussion

The following sections present and discuss the simulation results using the collision risk model described in Section 2. The simulations were conducted for several scenarios that the ATC might encounter in the airport environment with the current lack of UAS surveillance equipment (Section 4.1) and the possible incorporation of UAS detecting sensors in the near future (Section 4.2).

In particular, Section 4.1.1 presents the establishment of Alert Zones within terminal airspace that could assist the ATC to quickly evaluate if immediate mitigating action is needed for an incursion event, while Section 4.1.2 investigates the influence of different conflict-pair and Section 4.1.3 divide the Alert Zone with the expected time to collision to help with decision making. Finally, the comparison between deterministic and probabilistic Alert Zones are compared in Section 4.1.4 and the limitations of the Alert Zone setup explained in Section 4.1.5.

The possible methods that could be used to incorporate sensor data, likely available for terminal airspace in the near future, into the collision risk model presented before are described in Section 4.2.1, and the evaluation of these methods presented in Section 4.2.2 for false alert rate and the failure rate of the detection methods. These rates are also compared with those associated with the established system.

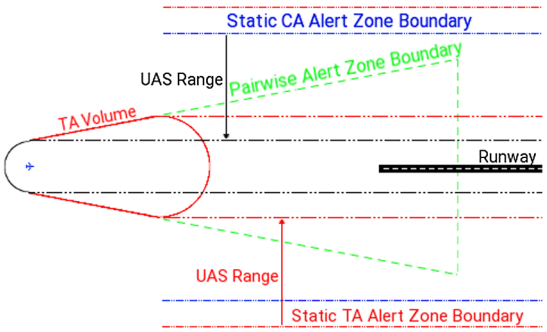

Fig. 6. Conceptual plot marking out the deterministic static (outer red and blue lines for TA and CA alert) and pairwise (green, extended from TA volume of the aircraft) Alert Zones boundaries relative to the runway and the protected volumes of a landing aircraft. The "UAS Range" is the maximum range of the UAS over the simulated period. (For interpretation of the references to colour in this figure legend, the reader is referred to the web version of this article.)

4.1. Static and pairwise alert zones

For collision risk assessment cases that does not involve the influence of external factors, such as ambient wind, the Alert Zones for UAS sighting could be established around the runway using the travel speed of the intruding UAS and the host aircraft. The concept of the Alert Zones layout is inspired by the creation of ACAS II protected volume, as shown out in Fig. 6. The conceptual zones from the figure were formed using a deterministic approach, which sketched out the Alert Zone boundaries using only the maximum travel range of the UAS, thus labeled as deterministic Alert Zones.

The Alert Zones could be further split into two types, the static Alert Zones and the pairwise alert zones, as labeled in Fig. 6. The static Alert Zones were constructed using the maximum travel distance of the UAS over the duration of the simulation, determined by the time needed by the aircraft to complete its operation within the terminal airspace. The pairwise Alert Zones were derived from the ACAS II protected volume concept, but utilized the time it took to complete the aircraft operation instead of the fixed time threshold of 20 s; this Alert Zone changes depending on the positions of the aircraft and the UAS at the start of the simulation.

4.1.1. Probabilistic alert zones

The probabilistic, static Alert Zone for a 70 s operation, as shown in Fig. 7, was established by connecting the initial UAS position that could result in greater than 50% of the UAS samples intruding into the protected area around the flight corridor; the dashed-line indicated regions without data points. The Alert Zone boundaries were established via an iterative process of placing the UAS at different initial "sighting" positions within the terminal airspace and assess the collision risk posed by the UAS under the assumption of worst-case "intention". To reduce the number of simulations required, the initial UAS position for each iteration would start out at along the corresponding deterministic Alert Zone boundaries and would be moved inward or outward depending on the collision assessment.

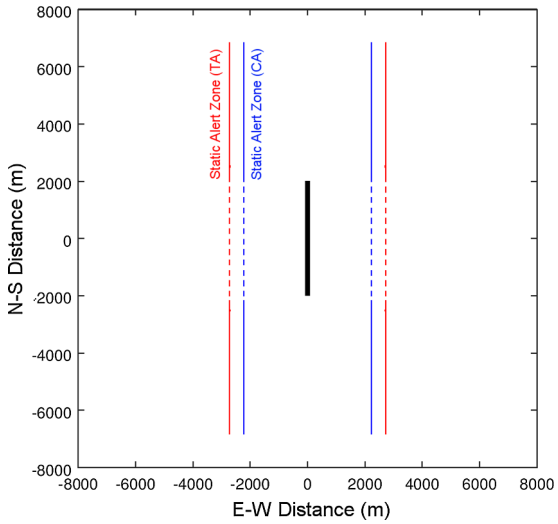

Fig. 7. Boundaries for probabilistic, static traffic advisory (TA) zone (red lines) and collision alert (CA) zone (blue lines). (For interpretation of the references to colour in this figure legend, the reader is referred to the web version of this article.)

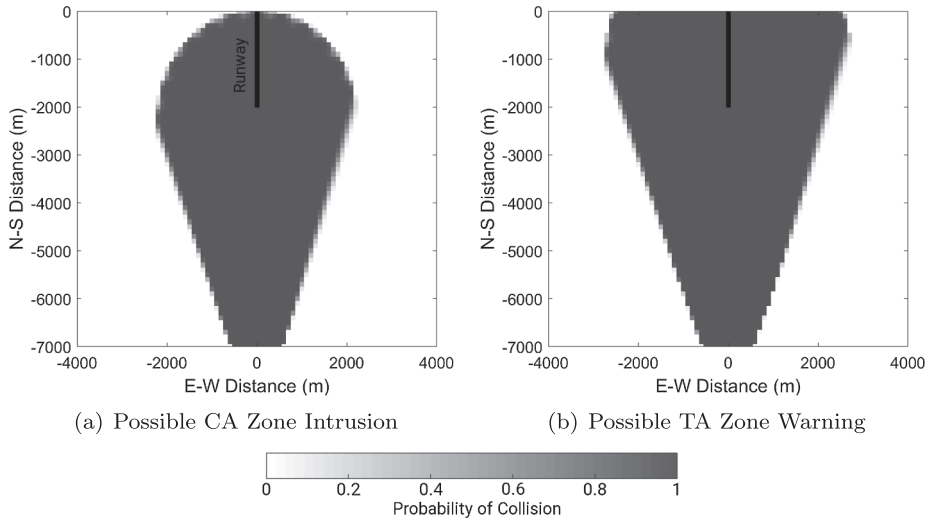

Fig. 8. Probabilistic pairwise collision assessment of initial UAS position that could lead to collision risk by intruding into (a) Collision Alert (CA) and (b) Traffic Advisory (TA) zones over the 70 s duration of the landing operation at 130 knots.

The static Alert Zones were setup such that the ATC would not need to know the exact position of the aircraft along the landing or takeoff corridor: an aircraft already in operation inside the terminal airspace should proceed as normal if the UAS is spotted outside of the alert zones; should the UAS be spotted inside the Alert Zones (on the relevant side of the runway), the pilot should be notified to take whatever action necessary to avoid a collision. Otherwise, the aircraft operation should be halted until the UAS has been removed from the airspace. The advantage of the static alert zone is the simplicity in setup and enforcement. The disadvantage is that the Alert Zones are specific to the type of UAS and aircraft used to establish the zones under calm atmospheric condition; the worst-case intent assumption for the UAS path prediction would also lead to false alarms and unnecessary disruption to air traffic operations.

The probabilistic, pairwise Alert Zones were established, based on conflict mapping in Ref. (Krozel et al., 1997; Yang and Kuchar, 1997), by first creating a mesh of initial UAS position, at fixed interval, surrounding the flight path of the aircraft. Collision risk assessments using 2000 samples Monte-Carlo simulations were then conducted at each of those positions for initial headings at 15° interval, and the highest collision risk predicted at that initial position was recorded. The resulting probability of collision using the two layers of protected volumes was visualized as scaled-color image. The established alert zones are specific to the aircraft-UAS pair in terms of landing speed for the aircraft and the maximum horizontal flight speed of the UAS. For the Alert Zone to account for the worst-case scenario, the aircraft would enter the terminal airspace at $t = 0$. Fig. 8 presents the pair-wise Alert Zone for initial UAS sightings, with the initial UAS positions laid out as a mesh covering an area of 8000 m by 7000 m with E-W interval of 200 m and N-S interval of 350 m; the simulations were conducted with 2000 samples with a duration of 70 s for each of the initial positions. The civil aviation aircraft is assumed to cross into the terminal airspace at $t = 0$. The figures showed that a difference UAS travel distance of around one grid length is sufficient for the collision risk to go from 0 to 1 close to the Alert Zone boundary.

Comparing to the Alert Zones for a landing aircraft, where the landing corridor/glide slope is fixed with similar landing speed, the creation of alert zones for a takeoff operation could be more complicated. The difference in aircraft type and takeoff weight would lead to different takeoff speed and runway length requirements, thus would need different Alert Zones to be created. Alternatively, the Alert Zone could be created using a regional airliner with shorter takeoff length and a slower takeoff speed as the “host” aircraft, which requires a larger Alert Zone. This could place the aircraft at (0,0) at $t = 0$ and travel at 130 knots following runway heading. Fig. 9 showed the Alert Zone for a regional jet with the takeoff speed of 140 knots. The impact of the difference in “host” aircraft travel speed on the Alert Zone boundary is further discussed in Section 4.1.2.

The pair-wise Alert Zones has the advantage of cover a smaller projected area, thus having a lower false alert rate comparing to the static Alert Zones. However, the creation of pair-wise Alert Zone for each conflict pairs would require the knowledge of the positions of both the “host” aircraft and the intruding UAS at the start of the simulation, either through real-time observations or UAS position estimation based on initial sighting reports. Both the static and pair-wise Alert Zones boundaries would change based on what is known about the UAS model and its flight performance, the effect of which would be discussed in Section 4.1.2.

In the case where the relative positions of the aircraft relative to the UAS is not precisely known, the pair-wise Alert Zone could be created with the assumption that the “host” aircraft enters (or become airborne) within the terminal airspace at $t = 0$ s. This way, an intruding UAS outside this Alert Zone boundaries would pose no threat to the aircraft already in operation in terminal airspace, regardless of its exact position (demonstrated in Section 4.1.3). Furthermore, an acceptable “worst-case” UAS velocity could be used to create the $t = 0$ pair-wise Alert Zone using either the Federal Aviation Administration (FAA) speed limit for small UAS or the maximum speed of small rotorcraft from the Association for Unmanned Vehicle Systems International (AUVSI) database. The subsequent aircraft that has yet to enter into the terminal airspace would need to suspend its operation unless a separate pair-wise Alert

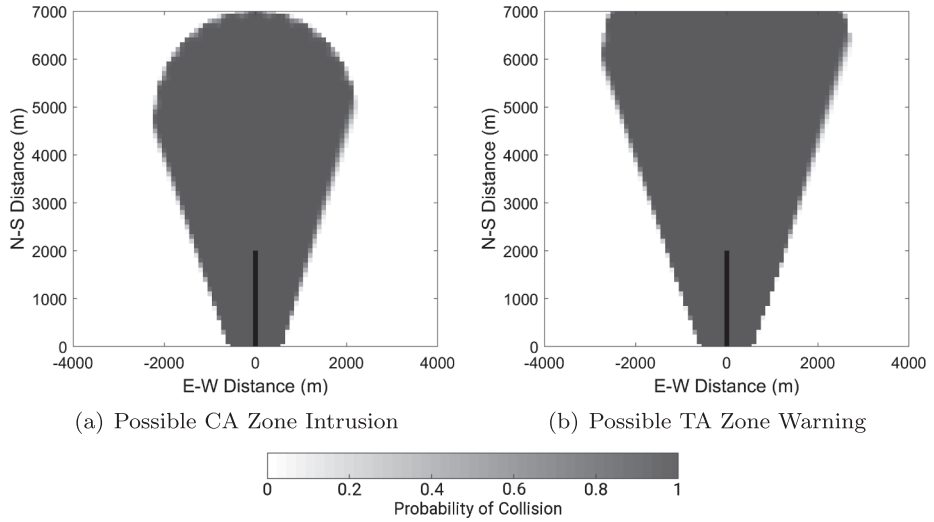

Fig. 9. Probabilistic pairwise collision maps for initial UAS position that could lead to incursion into (a) Collision Area (CA) and (b) Traffic Advisory (TA) zones over the simulation period for takeoff operation at 140 knots.

Zone could be established by the controller monitoring the UAS with handheld devices, e.g. binocular with range finder.

4.1.2. Sensitivity of alert zones to conflict pairs

The conceptual setup of the pair-wise Alert Zone (Fig. 6) suggests that the Alert Zone boundary is dependent on the flight performance of both the aircraft and the UAS in the conflict pair. As suggested in the previous section, a conflict pair involving a UAS and an aircraft with higher takeoff speed is expected have a narrower Alert Zone with steeper size slope compare to a pair with the same UAS but an aircraft with a slower takeoff speed. Alternatively, aircraft encounter with different UAS would also result in difference in the Alert Zone boundary.

A series of simulations were conducted to explore the Alert Zone resulting with different conflict pairs. This is conducted by first varying the takeoff speed of the aircraft while using the same UAS type as intruder; a second set of simulations were conducted for encounters between different UAS and an aircraft traveling at 140 knots.

Table 3 lists takeoff and landing speed from selected aircraft types that could be seen in Singapore. Simulations were conducted for takeoff operation with takeoff speed between 100 and 150 knots at 10 knots interval to serve as reference lines; all aircraft were assumed to have taken off at (0,0) to simplify the comparison of different Alert Zones.

DJI is one of the more popular manufacturers for recreational UAS in the world, making it easier to obtain the flight performance specifications needed for the Monte-Carlo model, either directly from the manufacturer's website or from third-party review sites. Table 4 presents a list of off-the-shelf recreational UAS, selected by the availability of their performance data; it covers UAS from pocket size selfie UAS to semi-professional-camera equipped UAS aimed at filmmakers. Note that kit-based UAS are not included due to the large variation in possible configurations, and could be anything from a small racing UAS weighting less than 0.5 kg to massive cargo hauling UAS that requires a permit to fly.

Simulations investigating the effect of aircraft travel speed were conducted using the specifications for Inspire 2 as intruder over a duration of 110 s; the simulation duration was increased to compensate for the longer time needed by the slower aircraft to exit the terminal airspace. Due to the number of variation tested, the simulations were conducted with 200 m intervals in the E-W Direction and 350 m in the N-S directions.

The simulation results from the influence of different aircraft speed are shown in Fig. 10(a), and match the expected outcome where faster aircraft speed results in a narrower Alert Zone. The results showed that the Alert Zone boundaries for the fastest and slowest aircraft could differ by as much as 1 km at the edge of the terminal airspace; the difference is much smaller (<500 m) if only aircraft with jet engines are considered. The TA and CA zone would have shown identical side-slope.

The results from simulations with different UAS types (Fig. 10(b)) showed that the side slope of the Alert Zones are also influenced

Table 3
Takeoff and Landing Speed for Selected Aircraft (Aircraft performance database, 2019).

Type	Takeoff Speed (knots)	Landing Speed (knots)
Regional Propeller (ATR-72)	110	120
Regional Jet (CRJ2)	135	140
Narrowbody (A321)	145	141
Widebody (A333)	140	140
Airbus 380–800 (A388)	150	140

Table 4
Performance Data for Selected UAS (DJI Technology Co., Ltd, 2017; Drone thrust testing, 2019).

UAS Model	M (kg)	T_{max} (kgf)	V_{max} (m/s)
DJI Inspire 2	3.4	8	26
DJI Phantom 3	1.3	3.2	20
DJI Mavic Pro	0.74	1.8	20
DJI Spark[a]	0.3	0.6	8.61

[a] Note that the controller range for Spark is less than 5 km.

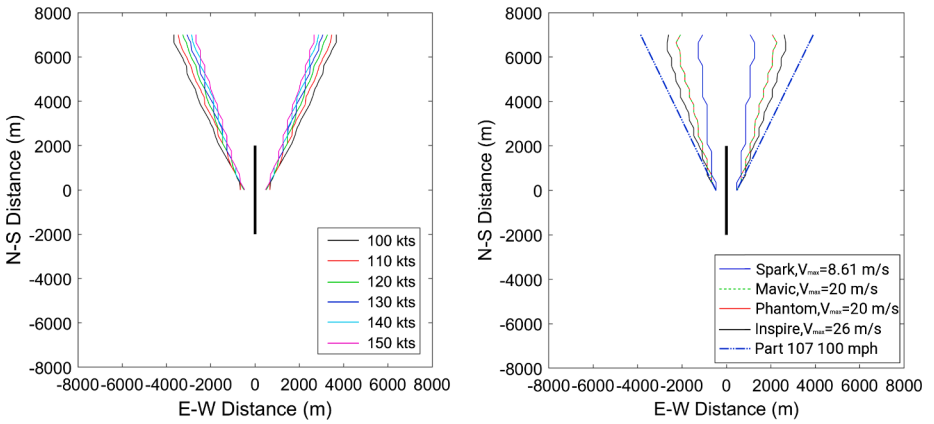

(a) Aircraft Travel Speed (b) Intruding UAS Type

Fig. 10. Probabilistic pairwise collision Alert Zone (using TA zone for collision assessment) with (a) Aircraft Travel Speed and (b) UAS Type over the takeoff operation (note that the lines for Mavic and Phantom overlaps).

by the maximum speed of the UAS. This is expected given the worst-case assumption; however, it appears that the maneuverability of the UAS does not play a discernible role when it comes to Alert Zone creation as seen from the boundaries for the Phantom and the Mavic. The lack of sensitivity of Alert Zone boundary to the UAS maneuverability is likely due to the enforcement of "worst-case intent." The deterministic boundary created using the FAA Part 107[4] speed limit was also included as an outer boundary for the Alert Zones.

4.1.3. Time delimited alert zones

The probabilistic pairwise Alert Zone could be further divided with the shortest estimated time to collision $\tau = r/V_{max}$ given that the positions of the "host" aircraft and the "intruder" are known at the beginning of the simulation. This would allow the ATC to have a better idea of instructions that could be sent to the pilot to help with avoiding the intruding UAS. The time-delimited Alert Zone for a "host" aircraft performing the landing operation and entering the 5 km airspace boundary at $t = 0$ s is shown in Fig. 11(a). Fig. 11(b) shows the time-delimited Alert Zone for an aircraft taking off with the assumption that it reaches takeoff speed at $t = 0$ s while crossing the (0,0) point (mid-runway). Additionally, the time-delimited Alert Zone for an aircraft performing landing operation that entered the terminal airspace 20 s before the time of UAS sighting is shown in Fig. 11(c).

Comparing to the Alert Zones described in Section 4.1.2, the implementation of time-delimited Alert Zone would require the availability of UAS detection equipment as it depends on knowing the relative positions of the "host" aircraft and the intruding UAS at the start of the simulation. The availability of the UAS detection equipment would also allow the creation of a more accurate pair-wise Alert Zone that does not assume the "host" aircraft to be at the terminal airspace boundary at $t = 0$ s for the landing case and (0,0) for the takeoff case. The comparison between Fig. 11(a) and (c) also demonstrated that the pair-wise Alert Zone created for $t = 0$ s entry time would fully encompass the Alert Zone of an aircraft that is already operating within the terminal airspace, thus could be used as a more conservative Alert Zone boundary for situation where the positions of the "host" aircraft and the UAS at $t = 0$ s are unknown.

With the evaluation of the estimated time to collision (τ), a list of ATC actions with different cutoff threshold could be created. The instructions issued by the ATC would depend on the human reaction time of the pilot and the mechanical reaction time of the aircraft. For example, the minimum total reaction time for the pilot and the aircraft after receiving the warning has been evaluated to be 3.88 s with standard deviation of 1.95 s in Ref. (Bagnall and Kay, 1975), or 5 s total in TCAS II logic (RCTA, 2013). Thus, mitigation action is unlikely for $\tau < 5$ s, and damage similar to that from a bird-strike for small recreational UAS (Olivares et al., 2017) could be expected. For 5 s $< \tau <$ 20 s, instructions for immediate avoidance maneuver should avoid a breach of the "host"

[4] 14 CFR §107.51 for small unmanned aircraft (under 55 lbs).

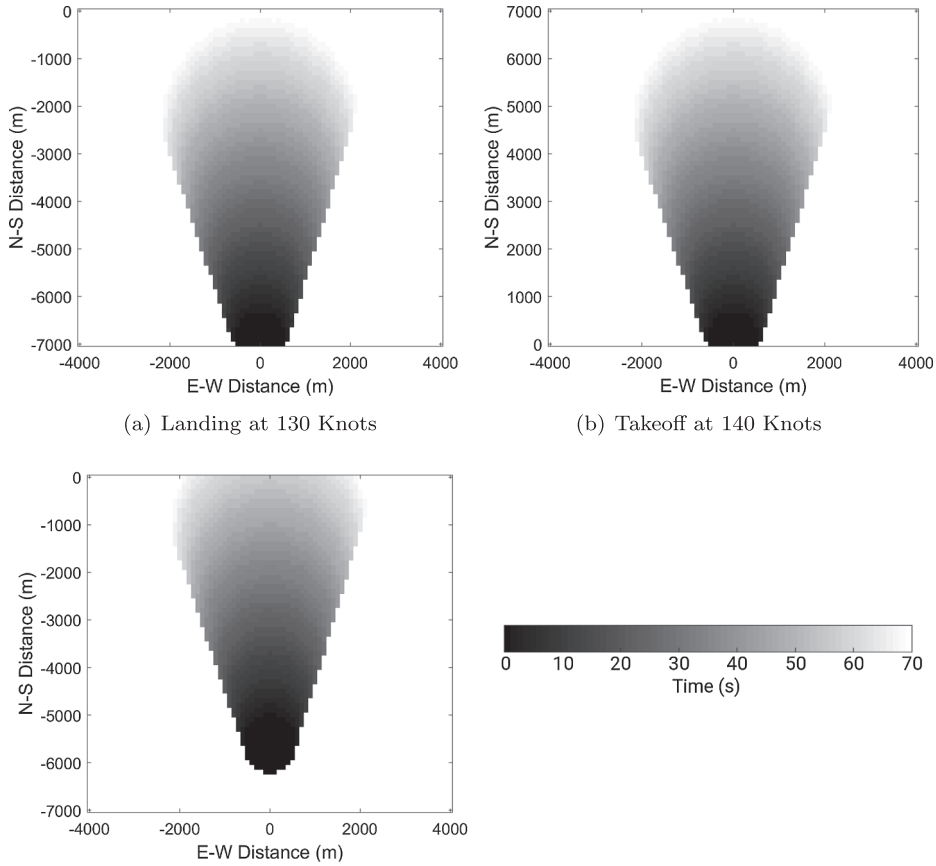

(a) Landing at 130 Knots (b) Takeoff at 140 Knots

(c) Early Entry for Landing

Fig. 11. Time delimited Alert Zone for τ (with the color bar on the bottom right) to reach 50% probability of collision for an aircraft performing (a) landing and (b) takeoff operation. (c) shows the Alert Zones for a landing aircraft that has already spent 20 s in the terminal airspace. (For interpretation of the references to colour in this figure legend, the reader is referred to the web version of this article.)

aircraft's protected volume. For collision pair with larger τ values, the pilot should have enough time to visually locate the intruder and take the necessary action to avoid a collision.

4.1.4. *Deterministic and probabilistic alert zones*

As mentioned in the introduction paragraph of Section 4.1, the deterministic Alert Zone could be created following Fig. 6 using the maximum speed of the UAS. Figs. 12 and 13 compares static and pair-wise Alert Zones created using the deterministic and

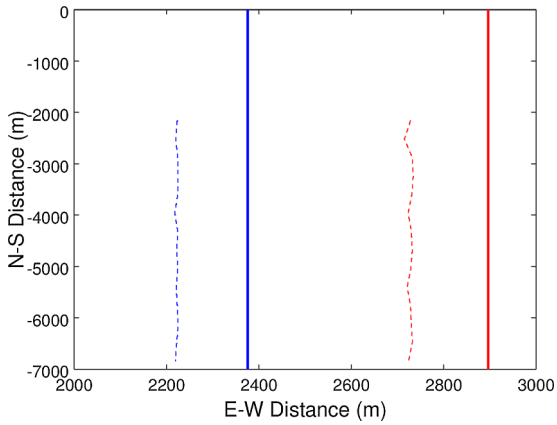

Fig. 12. Comparison between the deterministic and probabilistic boundaries for the static Alert Zones.

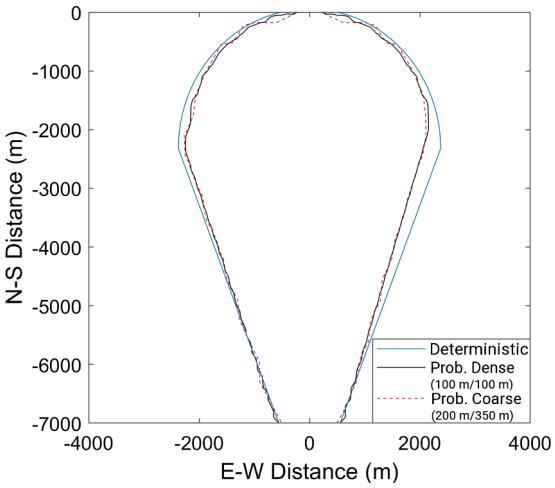

Fig. 13. Comparison between the deterministic and probabilistic (50% probability of collision, two interval sizes for initial positions) boundaries for pairwise Alert Zones for a landing aircraft at 130 knots and an intruder at 26 m/s.

probabilistic approach for an intruding UAS with performance described in Table 1.

The results from the static Alert Zones show ~200 m difference between the deterministic boundary and the probabilistic boundaries for 50% probability of collision. Fig. 13 from the pair-wise analysis shows a similar mismatch in the boundaries closer to the end of the track (thus a larger prediction time-frame and a larger τ), with a much closer matching between the deterministic and probabilistic boundaries closer to the entry point of the "host" aircraft. It also showed minimal difference between the contour line from the denser (100 m N-S, 100 m E-W intervals) and coarser (350 m N-S, 200 m E-W intervals) initial position grids. While the probabilistic boundary would generally be inside the deterministic boundary, the latter being created using the maximum speed of the UAS, though a few crossover points could be seen in Fig. 13. These crossover points showed that the probabilistic boundary exceed the deterministic boundary by <100 m, and are the result of the interpolation of collision probability over the intervals that was used for the UAS initial positions.

4.1.5. Limitations of the alert zones

The major limitation of both the deterministic and probabilistic Alert Zones is their dependency on knowing, or being able to estimate, the maximum speed of the intruding UAS. Without knowing the maximum speed of the UAS, the Alert Zone could be established using the maximum speed for small UAS required by the FAA or based on the data from the AUVSI database, as in the case of Ref. (Weinert et al., 2018b). The evaluation of the probabilistic Alert Zones, based on the current implementation, would also require significantly more computational time comparing to its deterministic counterpart while achieving a small reduction in the coverage size of the Alert Zone. Given the computational time requirement, the probabilistic Zones would need to be evaluated beforehand as a look-up table which covers the range of expected encounter pairs and ambient wind conditions.

Another limitation is specific to the Alert Zone evaluation model used in this study, which is its inability to modify the heading of the UAS, thus unable to properly account for the external factors such as crosswind. For example, the simulated UAS would not be able to ride the tailwind into the flight corridor, then reverse its direction of travel to remain within it. While increasing heading angle resolution might remove the gaps in the probability mapping, it would result in inaccurate minimum τ values for the associated initial position.

Furthermore, the implementation of time-specific pair-wise Alert Zone instead of the $t = 0$ s version would require some form of time-accurate UAS detection equipment. However, with the availability of such equipment, it might be more effective to perform real-time collision prediction instead, as discussed in Section 4.2. Note that while the proposed Alert Zone setup is limited in effectiveness due to the lack of available information on the intruder, the area covered by the Alert Zones where intervention is needed is still smaller than that of the current practice.

4.2. Augmentation with detection equipment

4.2.1. Incorporation of UAS tracking data

Assessment for collision prediction augmented by tracking data were carried out for the scenario of a UAS incursion into the terminal airspace where a commercial aircraft is conducting its landing operation. Based on the assumption that the airport is equipped with reliable UAS sensors, the sensor data was incorporated into the path prediction algorithm using two different methods: collision prediction using the assumption of worst-case intention (WCI Method), which assumes that the UAS will travel at full thrust towards the flight path; and the prediction where UAS travel direction from the sensor were used instead (the Direction Retention, or DR Method), where the path prediction takes the heading of the UAS from sensor data, and apply maximum available thrust to it. The tracked position of both UAS and the commercial aircraft were both assumed to be their true positions. Two different tracks were

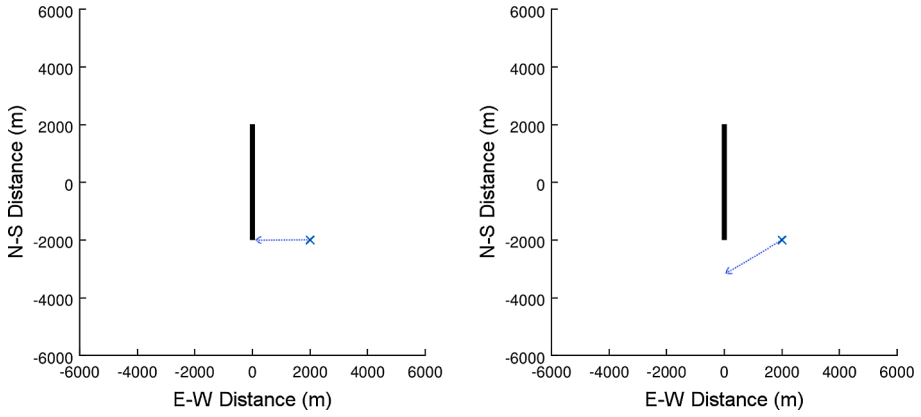

Fig. 14. Overview of the tracks taken by the intruding UAS: with (a) Heading 270° , and (b) Heading 240°.

used to illustrate the difference in prediction results, as illustrated in Fig. 14.

Track 1 (traveling with Heading 270°) takes the form of a simple straight line from the starting position towards the runway. In this case, simulations with both path prediction methods should result in identical collision risk profiles. Track 2 (traveling with Heading 240°), while also consisted of a straight line, would model the UAS with heading of 270° for the WCI Method, while the UAS would be modeled with a heading of 240° with the DR Method. For each path prediction methods, the UAS is assumed to be traveling with the maximum available thrust, or close to the 26 m/s maximum velocity of the UAS. Snapshots of the track 1 simulation results, which is identical in setup as the simulation conducted to establish the Alert Zones, are presented in Fig. 15 as snapshots over time. The "x" symbol marked the position of UAS as reported by the sensors, the light blue ellipse is the projected distribution of UAS position in 20 s, and the aircraft Alert Zones shown is based on the projected aircraft position 20 s from the time of sensor input. At 20 s from the start of simulation (Fig. 15(a)), the UAS is tracked to be at (1480, −2000). The path prediction simulation forecast that an incursion into the aircraft TA area would occur in the next 20 s. At 43 s from the start of simulation (Fig. 15(b), the UAS is at (882, −2000), which falls within the TA zone of the aircraft at the time of sensor report, which was shown in lighter color.

On the other hand, while the starting point of Track 2 is the same as Track 1, the warning for project incursion into TA zone was not predicted until 21 s after the start of the simulation, and only if the prediction was made using worst-case intention (the WCI Method) (Fig. 16). A small drift in the predicted UAS positions towards the reported direction of travel can be seen in prediction using the WCI Method. This is because no thrust was provisioned to counter the initial velocity to maintain a straight path, as that would increase the time-to-collision. Further along the track, the predicted TA zone incursion risk would slowly drop off until <50% of the sample falls within the TA zone. By 40 s after the start of the simulation, simulations using both prediction method showed that the UAS would pass behind the airplane without posing a hazard (Fig. 17).

Note that no collision between the UAS and the landing aircraft occurred with the Track 2 even though the TA warning was triggered using the WCI Method. However, the TA warning that was triggered at $t = 21$ s actually indicated that the UAS might intrude into the TA zone in 20 s (at $t = 41$ s), which in turns indicated that the UAS might intrude into CA zone in another 20 s (at

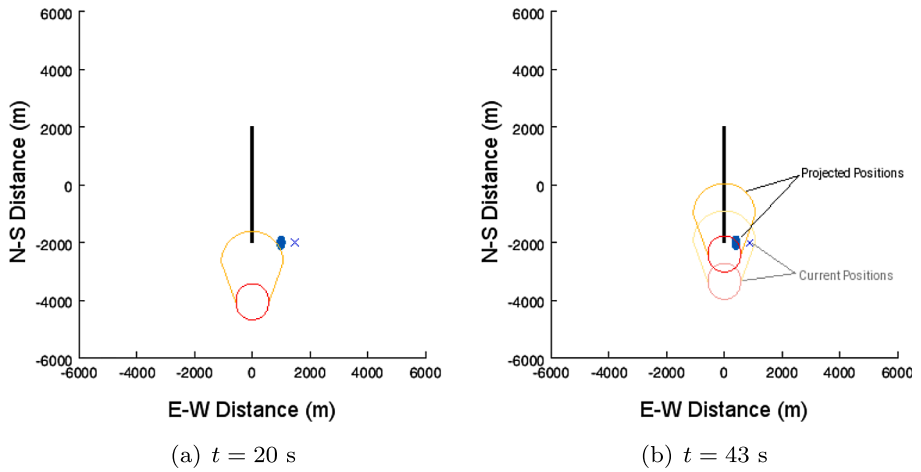

Fig. 15. Projection of UAS and aircraft position 20 s into the future predicting the triggering of (a) TA warning (at $t = 20$ s) and (b) CA warning (at $t = 43$ s).

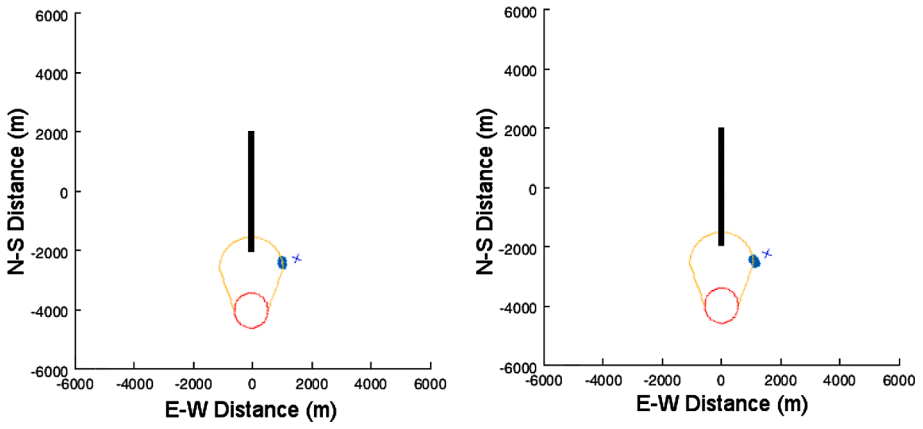

(a) the WCI Method (b) Direction Retention Method

Fig. 16. The difference in collision assessment approach led to difference in collision prediction at $t = 21$ s, as (a) the WCI Method triggered the TA alert, while (b) Direction Retention Method did not.

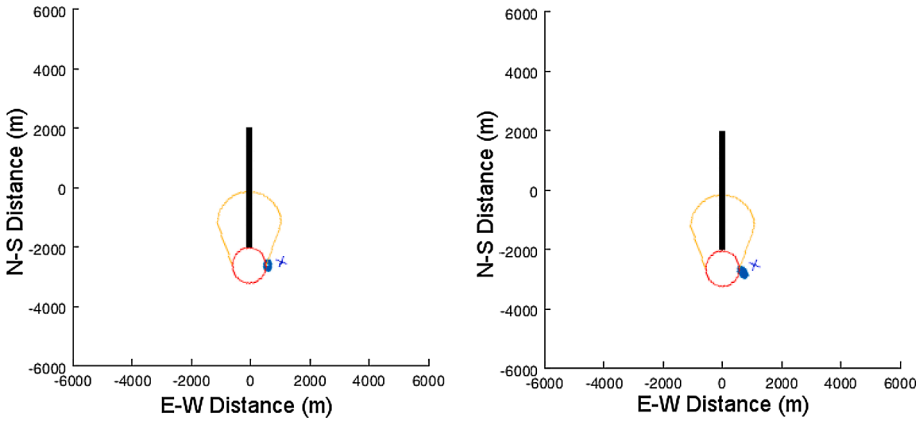

(a) the WCI Method (b) Direction Retention Method

Fig. 17. At $t = 40$ s, neither (a) prediction using the CPA method, nor (b) prediction with last known direction of travel, forecast a collision within the next 20 s.

$t = 61$ s) if a direct path towards the flight corridor at maximum speed is maintained. Assuming that the ACAS time modifier of 20 s specified in ACAS is the maximum amount of time allocated to the pilots to execute collision prevention maneuvers, the function of the TA zones in the simulation would overlap the function of the 20 s UAS position forecast but with lower accuracy. The path prediction methods could be further extended to incorporate the instantaneous speed of the UAS, if available. In that case, the sensor would provide the position, heading, and speed information (the PHS Method) of the UAS to the collision risk model. However, given the test track setup presented above, it would produce the same prediction result as the one from the DR Method.

4.2.2. Influence of the sensor data availability

Randomly generated UAS tracks were used as the sensor input to further test the collision risk assessment algorithm. The randomized UAS track generator was based on the path prediction algorithm used in the Monte-Carlo simulation. The travel intent of the UAS is no longer enforced in the track generation, and randomized initial conditions were used; at each time step, a normal distribution was used to determine the speed and direction of travel, with the values from the previous time-step as mean of the distribution and a variance of 0.04. A collection of 10 sample tracks using the test track generator are shown in Fig. 18. For a landing aircraft with operation time of 70 s, the sensor-based collision prediction algorithm would only be run until the $t = 50$ s data point. This is because any collision predicted after that time would most likely occur after the aircraft has safely landed, depending on the prediction method used. A pair-wise CA Alert Zone was generated for the entire 70 s operation time for comparison.

The evaluation of warnings issued by sensors based path prediction methods comparing to those issued based on Alert Zones established earlier was conducted using 1000 sample tracks. The initial positions of those tracks were randomly generated inside the

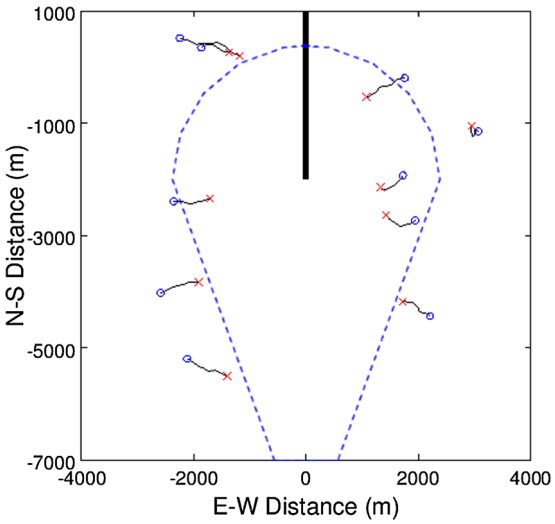

Fig. 18. Examples of random tracks generated to serve as sensor input. The blue dotted line indicated the boundary of the deterministic pair-wise Alert Zone. (For interpretation of the references to colour in this figure legend, the reader is referred to the web version of this article.)

deterministic, static Alert Zone with the exception of the ~1000 m[5] closet to the runway center-line, as the UAS would have a high likelihood of triggering a collision warning as soon as the simulation starts using the WCI Method. Of the 1000 samples tracks generated, 100% of the initial positions fall inside the deterministic, static Alert Zone, while ~46% would fall within the deterministic, pair-wise alert zone[6] based on its area. The deterministic Alert Zones are used for illustrative purposes only, and chosen for their simpler geometry and ease of implementation into the existing code.

Fig. 19 displays the initial positions of the sample tracks in relation to the pair-wise Alert Zone. The markers for these initial positions were colored based on the predicted chance of collision, i.e. the ratio of samples that falls into the CA zone of the airplane from a 20 s Monte-Carlo prediction based on sensor inputs. Table 5 tallied the number of samples initiated in the pair-wise Alert Zone, the number of sample tracks that resulted in the CA intrusion warning (total warnings and warnings issued before $t = 50$ s), the number of sample tracks that would lead to an "Actual Collision" (as in CA zone intrusion) if both the aircraft and the UAS remains on their track. Note that all tracks that led to an "Actual Collision" received a CA warning beforehand.

The number of samples with initial position inside the pair-wise alert area could be used to show the statistical variation that should be expected from the simulation results. From the sample of 1000 per simulation run, 48.5%, 48.8%, and 46.8% of the sample tracks would trigger collision warning under pair-wise Alert Zone based system; the mean value from the three simulation runs is 48.03% of samples falling within the pair-wise alert area, which is slightly higher compared to the expected pair-wise alert area warning trigger rate of 46%. An increase in number of sample tracks would be required to reduce this difference and improve statistical accuracy of the other measurements.

Since all "Actual Collision" from the simulation runs received a CA warning ($t \leqslant 50$ s) beforehand, the difference between the number of CA warnings issued before $t = 50$ s and the total CA warning issued is the number of predicted collisions that would not take place until the aircraft has landed, i.e. false positive warnings. Of the three methods used, only the WCI Method could guarantee that no collision would happen in this operation if no CA warning was issued before $t = 50$ s; using the other two methods a sudden speed-up by the UAS that would result in a non-zero chance of false negative prediction. Overall though, the ratio of false positive warning from the WCI Method with reduced monitor time is about the same as the ratio from the PHS Method without such reduction.

In a sense, the three prediction methods could be view as collision assessment based on different availability of reliable UAS tracking data. The WCI Method would correspond to a sensor that could reliably detect the position of the UAS for the two-second update interval used in the simulation, but not the instantaneous speed and direction of the UAS; the DR Method could be from a sensor that could detect accurate heading of the UAS but not the speed; and the PHS Method would be for a sensor with a high enough scan rate to obtain data for all three variables.

Using the mean Bayes Estimator for zero-failure data (Bailey, 1997), the probability of failure for the sensor-based prediction is $\hat{p} = 1/(1000 + 2) = 9.98 \times 10^{-4}$. Based on the probability of failure for the sensor based on the detection rate of 99%, the overall estimated probability of failure for collision alert, given the available data, is around 10^{-5}. In other words, even without accounting for sensor measurement errors, the available simulation data does not have sufficient samples to produce an estimated probability of failure that meets the requirement (10^{-7} failure rate) for civil aviation applications.

Further simulations were carried out with all three methods for 10,000 sample tracks to assess the failure rate of the collision

[5] Width of TA zone: DMOD + $V_{uas,max} \times 20$ s.

[6] For a landing aircraft landing at 140 knots and the UAS used in previous simulations.

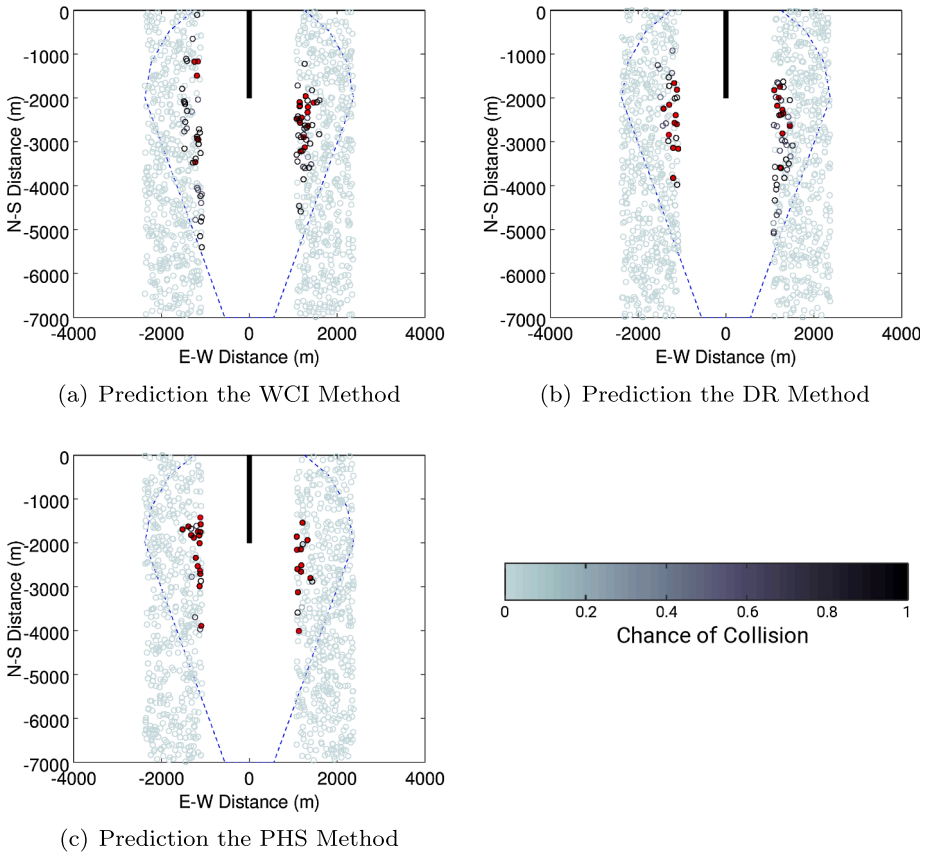

(a) Prediction the WCI Method

(b) Prediction the DR Method

(c) Prediction the PHS Method

Fig. 19. Evaluation of collision warning issued by systems using the three path prediction methods. Markers are the initial positions colored (with the color-bar on the bottom right) based on the maximum collision risk predicted before $t = 50$ s; markers with tracks that intrude into the CA zone before $t = 70$ s are filled. (For interpretation of the references to colour in this figure legend, the reader is referred to the web version of this article.)

Table 5
Alert Results from 1000 Simulated UAS Tracks.

Variable	WCI Method	DR Method	PHS Method
Inside Pairwise Alert Area	485	488	468
CA Warning ($t \leqslant 50$ s)	77	64	36
Total CA Warning Issued	135	123	78
CA Zone Incursion	20	21	27

Table 6
Alert results from 10,000 Simulated UAS Tracks.

Variable	WCI Method	DR Method	PHS Method
Inside Pairwise Alert Area	4645	4666	4615
CA Warning ($t \leqslant 50$ s)	706	655	270
CA Zone Incursion	202	248	222
Collision without Warning	0	0	3
Estimated Failure Rate	9.99×10^{-5}	9.99×10^{-5}	3.99×10^{-4}
False Alarm Rate	71.38%	62.14%	18.89%

prediction models. The simulation results are shown in Table 6 along with the estimated failure rate and the false alarm rate for the two prediction methods used.

The simulation results showed that collision prediction with the PHS Method has a probability of failure of 3.99×10^{-4}, along with an 18.89% false alarm rate. On the other hand, while the probability of failure for either of the WCI and the DR Method is much lower at 9.99×10^{-5}, and could be rated even lower if more simulations were conducted. However, the resulting false alarm rate with the WCI Method is much higher at 71.38% compared to the 18.89% from the PHS Method. That is to say, only 1 in 4 alert issued by

collision prediction the WCI Method would result in the loss of well-clear, which would create an excess of nuisance alerts and lead to a loss in effectiveness of the warning system. For real world examples, the available data suggested that the false alert rate for "TCAS" is at 10% and the user request evaluation tool (URET) for air route traffic control is at 50% (Rantanen et al., 2004).

For better perspective with the failure rate, the bird and wildlife strike reported by the FAA in 2016 is 30.92 reported incidents per 100,000 commercial air carrier movements, of which 1.42 reported unspecified amount of damage to the aircraft (Dolbeer and Begier, 2017). Assuming that a commercial aircraft were designed to survive a bird and wildlife strike from the above statistics and still stays within the 1×10^{-9} fatality rate threshold, the acceptable combined failure rate for the UAS sensors and alert system would be 3.092×10^{-4} for UAS collision. This could imply that predicting UAS collision with the PHS Method could result in an acceptable failure rate as well as false alarm rate when combined with the failure rate of the sensors. However, this number does not account for the mass difference between the bird and the UAS in this study, as well as the difference in damage caused by the bird and the UAS (Olivares et al., 2017). It also does not discriminate between UAS strike on critical and non-critical aircraft components.

5. Conclusion

Investigations were carried out to evaluate different methods used to mitigate collision risk posed by an intruding UAS within the terminal airspace, with or without the installation of UAS detection equipment. The simulations conducted were limited to the aircraft that is already within the terminal airspace after the initial report of UAS sighting, and all subsequent flight operations are assumed to be suspended until the safety hazard no longer exist, either as a collision risk or as foreign object debris. The simulations were also limited to 2D using a simplified equation of motions that assumed constant acceleration during each time step. For collision risk management without sensors for UAS tracking, two different Alert Zone setups, the static and the pair-wise Alert Zones, were proposed. In the cases where UAS tracking data is available, three different path prediction methods were tested for their false positive and false negative rates.

The Alert Zones setup could provide a relatively straight forward way for the air traffic controllers to determine if an intruding UAS would pose an immediate threat to the safety of the airport operation. While the static Alert Zone does not account for the positional difference between the UAS and the aircraft in operation, it still covers a smaller region than the current 5 km exclusion zone while minimizing the collision risk posed by the UAS on the aircraft. The pair-wise Alert Zone could further reduce the region of the terminal airspace where immediate action would need to be taken, thus a reduction in false alert. The "$t = 0$" pair-wise Alert Zone, with the assumption of speed limit based on UAS type, could be utilized for airport without dedicated UAS detection equipment to maintain aircraft safety while reducing disruptions as compared to the current setup. Simulations were also conducted to investigate the influence of different aircraft takeoff speed and UAS type on the Alert Zone boundary. The results showed that aircraft with higher takeoff speed would require a smaller Alert Zone, while UAS top speed appeared to be the only factors being investigated that would impact the Alert Zone sizing. Therefore, the effectiveness of the Alert Zone would be limited by the knowledge, or lack thereof, of the intruder's maximum speed. Additionally, the Alert Zone boundaries could be useful to airport authorities for determining portion of the airspace to prioritize UAS sensor installation.

The investigation with the sensor-based collision prediction showed that the availability of tracking data has the potential to reduce the rate of false collision warning for the aircraft operating in the terminal airspace. Of the three methods tested under the assumption of no influence by external factors, the simulation results suggested that the PHS Method, which predict the future UAS position distribution by maintaining its speed and travel direction from sensor measurements, have the lowest chance of issuing a false positive warning. This is in-line with the expectation that, for the simplified system presented in this paper, more information available to the collision assessment model would result in a more accurate prediction. Additional simulations with a larger data set of 10,000 sample tracks showed that path prediction with the PHS Method exhibits a failure rate of 3.99×10^{-4} with a false alert rate of 18.89 %.

Acknowledgments

The work on"Collision Risk Modeling" is a part of the Traffic Management - Unmanned Aerial Systems (TM-UAS) program funded by the Air Traffic Management Research Institute (ATMRI) in the Nanyang Technological University (NTU), Singapore. The authors would like to thank Ms. Lynette Koay Jie Ting for her help in code development and testing.

Appendix A. Supplementary material

Supplementary data associated with this article can be found, in the online version, at https://doi.org/10.1016/j.trc.2019.09.017.

References

Air Navigation Order, 2018. Civil Aviation Authority of Singapore, September, 2018. Unmanned Aircraft Operations and Activities, PART XA.
Aircraft performance database (Accessed Jan, 2019). <https://contentzone.eurocontrol.int/aircraftperformance/>.
Angelov, P. (Ed.), 2012. Sense and Avoid in UAS: Research and Applications. John Wiley & Sons, Hoboken, NJ, U.S.A..
FAA, 2014. Automatic Dependent Surveillance-Broadcast (ADS-B) Flight Inspection. Federal Aviation Administration, Washington D.C., U.S.A.
BBC News, 2017. Drone causes gatwick airport disruption, BBC. <http://www.bbc.com/news/uk-40476264>.

Bagnall, J.J., Kay, I.W., 1975. Review and analysis of some collision avoidance algorithms with particular reference to antc-117, Tech. Rep. FAA-RD-75-72. Federal Aviation Administration, Washington D.C., U.S.A.
Bailey, R.T., 1997. Estimation from zero-failure data. Risk Anal. 17 (3), 375–380.
Carpenter, B.D., Kuchar, J.K., 1997. Probability based collision alerting logic for closely-spaced parallel approach. In: 35th Aerospace Sciences Meeting and Exhibit. American Institute of Aeronautics and Astronautics, Reno, NV, U.S.A. https://doi.org/10.2514/6.1997-0222.
Chen, Y.F., Liu, M., Everett, M., How, J.P., 2017. Decentralized non-communicating multiagent collision avoidance with deep reinforcement learning. In: 2017 IEEE International Conference on Robotics and Automation (ICRA), pp. 285–292. https://doi.org/10.1109/ICRA.2017.7989037.
Cone, A.C., Thipphavong, D.P., Lee, S.M., Santiago, C., 2017. UAS well clear recovery against non-cooperative intruders using vertical maneuvers. In: 17th AIAA Aviation Technology, Integration, and Operations Conference, Colorado, USA.
Cook, S.P., Brooks, D., Cole, R., Hackenberg, D., Raska, V., 2015. Defining well clear for unmanned aircraft systems. In: AIAA SciTech Forum, Kissimmee, FL, U.S.A. https://doi.org/10.2514/6.2015-0481.
Davies, J., Wu, M.G., 2013. Comparative analysis of ACAS-Xu and DAIDALUS detect and avoid system. Tech. Rep. NASA/TM-2018-219773, NASA Ames Research Center, Moffett Field, CA, U.S.A.
Deulgaonkar, P., 2017. Shutting down Dubai International Airport due to a drone costs $100,000 a minute, Arabian Business. <http://www.arabianbusiness.com/content/375851-drone-costs-100000-minute-loss-to-uae-airports>.
DJI Technology Co., Ltd, Inspire 2 User Manual, 1st Edition, SZ DJI Technology Co. Ltd, Shenzhen, China, 2017.
Dolbeer, R.A., Begier, M.J., 2017. Wildlife strike to civil aircraft in the United States 1990–2016, Tech. Rep. Serial Report Number 23, 2017.
Drone thrust testing (Accessed Jan, 2019). <https://www.halfchrome.com/drone-thrust-testing/>.
Duffield, M.O., McLain, T.W., 2017. A well clear recommendation for small UAS in high-density, ADS-B-enabled airspace. In: AIAA SciTech Forum. Grapevine, TX, U.S.A. https://doi.org/10.2514/6.2017-0908.
EUROCONTROL (Ed.), 2016. ACAS Guide: Airborne Collision Avoidance Systems (incorporating TCAS II versions 7.0 & 7.1 and introduction to ACAS X), second ed., European Organisation for the Safety of Air Navigation, Brussels, Belgium.
Fasano, G., Accardo, D., Moccia, A., Carbone, C., Ciniglio, U., Corraro, F., Luongo, S., 2008. Multi-sensor-based fully autonomous non-cooperative collision avoidance system for unmanned air vehicles. J. Aerosp. Comput., Inform., Commun. 5 (10), 338–360.
Fasano, G., Accardo, D., Tirri, A.E., Moccia, A., Lellis, E.D., 2015. Radar/electro-optical data fusion for non-cooperative UAS sense and avoid. Aerosp. Sci. Technol. 46, 436–450. https://doi.org/10.1016/j.ast.2015.08.010.
Feng, Q., Liu, Y., Zhu, Z.H., Hu, Y., Pan, Q., Lyu, Y., 2018. Vision-based relative state estimation for a non-cooperative target. In: 2018 AIAA Guidance, Navigation, and Control Conference, Florida, USA.
George, T., 2018. Video shows drone coming close to plane landing at McCarran, KTNV. <https://www.ktnv.com/news/video-shows-drone-coming-close-to-plane-landing-at-mccarran>.
Hall, T., Soares, M., 2008. Analysis of localizer and glide slope flight technical error. In: 2008 IEEE/AIAA 27th Digital Avionics Systems Conference, 2008, pp. 2.D.2–1–2.D.2–9. https://doi.org/10.1109/DASC.2008.4702786.
Manual on Airspace Planning Methodology for the Determination of Separation Minima, 1st ed. International Civil Aviation Organization.
Inspire 2 (Accessed Jan, 2019). <https://www.dji.com/inspire-2>.
Johnson, M., Mueller, E.R., Santiago, C., 2015. Characteristics of a well clear definition and alerting criteria for encounters between UAS and manned aircraft in class e airspace. In: Eleventh USA/Europe Air Traffic Management Research and Development Seminar (ATM2015), 2015.
Kim, K.-Y., Park, J.-W., Tahk, M.-J., 2007. UAV collision avoidance using probabilistic method in 3-d. In: 2007 International Conference on Control, Automation and Systems, pp. 826–829. https://doi.org/10.1109/ICCAS.2007.4407015.
Kochenderfer, M.J., Chryssanthacopoulos, J.P., 2011. Robust Airborne Collision Avoidance through Dynamic Programming, no. ATC-317, Lincoln Laboratory. Massachusetts Institute of Technology, Lexington, MA, U.S.A.
Kochenderfer, M.J., Edwards, M.W., Espindle, L.P., James, K.K., Griffith, J.D., 2010. Airspace encounter models for estimating collision risk. J. Guid., Control Dynam., vol. 33, 2.
Krozel, J., Peters, M.E., Hunter, G., 1997. Conflict detection and resolution for future air transport management. Tech. Rep. NASA-CR-97-295944, NASA Ames Research Center, Moffett Field, CA, U.S.A.
Kuchar, J.K., Yang, L.C., 2000. A review of conflict detection and resolution modeling methods. IEEE Trans. Intell. Transport. Syst. 1 (4), 179–189.
Lee, S.M., Park, C., Johnson, M.A., Mueller, E.R., 2013. Investigating effects of well clear definitions on UAS sense-and-avoid operations in enroute and transition airspace. In: 2013 Aviation Technology, Integration, and Operations Conference, Los Angeles, CA, 2013. https://doi.org/10.2514/6.2013-4308.
Looze, D., Plotnikov, M., Wicks, R., 2016. Current Counter-drone Technology Solutions to Shield Airports and Approach and Departure Corridors. Tech. rep.. Massachusetts Department of Transportation, Boston, MA, U.S.A.
McFadyen, A., Martin, T., 2016. Terminal airspace modeling for unmanned aircraft systems integration. In: International Conference for Unmanned Aircraft Systems, pp. 789–794.
McFadyen, A., Martin, T., Mejias, L., 2016. Simulation and modeling tools for quantitative assessments of unmanned aircraft systems and operations. In: IEEE Aerospace Conference.
Metz, I.C., Ellerbroek, J., Muḧlhausen, T., Kuler, D., Hoekstra, J.M., 2017. Simulating the risk of bird strike. In: Seventh SESAR Innovation Days, Belgrade, Serbia, 2017.
Michel, A.H., Gettinger, D., 2015. Drone sightings and close encounters: An analysis, Tech. rep., Center for the Study of the Drone, Annandale-on-Hudson, NY, U.S.A.
Miller, R.G., 1974. The jackknife - a review. Biometrika 61 (1), 1–16. https://doi.org/10.1093/biomet/61.1.1.
Muller, E., Kochenderfer, M.J., 2016. Simulation comparison of collision avoidance algorithms for small multi-rotor aircraft. In: AIAA Modeling and Simulation Technologies Conference, 2016. https://doi.org/10.2514/6.2016-3674.
Muñoz, C.A., Narkawicz, A., Chamberlain, J., Consiglio, M., Upchurch, J., 2014. A family of well-clear boundary models forthe integration of UAS in the nas. In: 14th AIAA Aviation Technology, Integration, and Operations Conference, 2014. https://doi.org/10.2514/6.2014-2412.
Olivares, G., Gomez, L., de los Monteros, J.E., Baldridge, R.J., Zinzuwadia, C., Aldag, T., 2017. Volume II - UAS airborne collision severity evaluation - quadcopter, Tech. Rep. DOT/FAA/AR-xx/xx, National Institute for Aviation Research.
Otero, S.D., Barker, G.D., Jones, D.R., 2013. Initial concept for terminal area conflict detection, alerting, and resolution capability on or near the airport surface, version 2.0. Tech. Rep. NASA/TM-2013-218052, NASA Langley Research Center, Hampton, VA, U.S.A. 2013.
Paielli, R.A., Erzberger, H., 1997. Conflict probability estimation for free flight. J. Guid., Control, Dynam. 20 (3), 588–596.
Peinecke, N., Kuenz, A., 2017. Deconflicting the urban airspace. In: 2017 IEEE/AIAA 36th Digital Avionics Systems Conference, St. Petersburg, FL, U.S.A., 2017. https://doi.org/10.1109/DASC.2017.8102048.
Rantanen, E.M., Wickens, C.D., Xu, X., Thomas, L.C., 2004. Developing and validating human factors certification criteria for cockpit display of traffic information avionics. Tech. Rep. AHFD-04-1/FAA-04-1, 2004.
Minimum operational performance standards for traffic alert and collision avoidance system (tcas ii) airborne equipment, Tech. Rep. RTCA/DO-185B, 2013.
Taylor, D.H., 1990. Uncertainty in collision avoidance maneuvering. J. Navig. 43 (2), 238–245.
Tony, L.A., Ghose, D., Chakravarthy, A., 2017. Avoidance maps: a new concept in UAV collision avoidance. In: 2017 International Conference on Unmanned Aircraft Systems (ICUAS), https://doi.org/10.1109/ICUAS.2017.7991382.
Verstraeten, J.G., Stuip, M., van Birgelen, T.M., 2012. Assessment of detect and avoid solutions for use of unmanned aircraft systems in nonsegregated airspace, Tech. Rep. NLR-TP-2012-494, NLR Air Transport Safety Institute, Amsterdam, The Netherlands.
Wang, C.H.J., Tan, S.K., Ting, L.K.J., Low, K.H., 2018. Impact of sensors on collision risk prediction for non-cooperative traffic in terminal airspace. In: International Conference for Unmanned Aircraft Systems, Dallas, TX, U.S.A., 2018, 9 pages. https://doi.org/10.1109/ICUAS.2018.8453424.
Weinert, A., Underhill, N., 2018. Generating representative small UAS trajectories using open source data. In: 2018 IEEE/AIAA 37th Digital Avionics Systems Conference, London, United Kingdoms, 2018. https://doi.org/10.1109/DASC.2018.8569745.
Weinert, A.J., Harkleroad, E.P., Griffith, J.D., Edwards, M.W., Kochenderfer, M.J., 2012. Uncorrelated Encounter Model of the National Airspace Version 2.0, no. ATC-404, Lincoln Laboratory, Massachusetts Institute of Technology, Lexington, MA, U.S.A., 2012.
Wallace, R.J., Kiernan, K.W., Haritos, T., Robbins, J., D'souza, G.V., 2018a. Evaluating small UAS near midair collision risk using AeroScope and ADS-B. Int. J. Aviat., Aeronaut.,

Aerospace, vol. 5, 4.
Weinert, A., Campbell, S., Vela, A., Schuldt, D., Kurucar, J., 2018b. Well-clear recommendation for small unmanned aircraft systems based on unmitigated collision risk. J. Air Transport., vol. 26, 3. https://doi.org/10.2514/1.D0091.
Yang, L.C., Kuchar, J.K., 1997. Prototype conflict alerting system for free flight. J. Guid., Control, Dynam. 20 (4), 768–773.
Yang, L.C., Kuchar, J.K., 1998. Using intent information in probabilistic conflict analysis. In: Guidance, Navigation, and Control Conference and Exhibit. American Institute of Aeronautics and Astronautics, Boston, MA, U.S.A. https://doi.org/10.2514/6.1998-4237.
Zhang, Y., Shortle, J., Sherry, L., 2010. Comparison of arrival tracks at different airports. In: 4th International Conference on Research in Air Transportation, pp. 481–486.